

MULTISPECIES SIMULATION OF THE FRIB FRONTEND NEAR THE ECR SOURCES WITH THE WARP CODE

K. Fukushima*, S. M. Lund, FRIB, Michigan State University, MI 48824, USA
C. Y. Wong, NSCL, Michigan State University, MI 48824, USA

Abstract

The linear accelerator in the Facility for Rare Isotope Beams (FRIB) will use Electron Cyclotron Resonance (ECR) sources. ECR sources generate a high-brightness DC beam with high charge states. However, the ECR sources produce numerous species that must be collimated to one or two target species with minimal degradation in beam quality. The first stage of this collimation is accomplished in a tight 90° dipole bend with a wide aperture and slanted pole faces to provide additional focusing. We report on simulations carried out with the Warp PIC code [1–3] for operation with high-rigidity Uranium ions. These simulations use linked 2D xy-slice runs in the straight section upstream of the bend and steady-state 3D simulations in the dipole bend. Simulations with ideal (sector) and full 3D field maps of the dipole magnet are contrasted. Issues associated with placing a 3D dipole field with an extended fringe field on a bent coordinate system are addressed. Placement of the dipole bend is optimized consistent with the 3D field and is found to closely correspond to the ideal field center. Minimal problems are found (small centroid shift and distribution distortions) due to 3D space charge effects in the initial species separation within the bend when using simple fractional neutralization factors in the anticipated range.

INTRODUCTION

In the FRIB front-end, diagnostic systems are limited due to the source operating on a high-voltage stand and the many-species beam distribution emerging from ECR source being DC. Therefore it is desirable to develop improved numerical models to better understand uncertainties and support front-end commissioning.

SIMULATION DESCRIPTION

Lattice

Figure 1 (upper panel) shows the front-end lattice from the ECR source through the first bending magnet and (lower panel) the corresponding axial magnetic (from ECR and solenoids; blue) and electrostatic (from grating gap; red) axial accelerating fields in straight section. Parameters of the two solenoids and one electrostatic (ES) gap are listed in Table 1. These elements have short length with wide apertures, so nonlinear fields are significant. Note that fringe fields neighboring elements can overlap — particularly the ECR and the first solenoid. Fields of these elements are calculated in 2D by the finite element codes LORENTZ [4]

(ECR solenoids) and Poisson [5] (iron solenoids and ES gap) and imported on a high-resolution r - z mesh.

Table 1: Lattice Element Parameters

Component	Length [cm]	Aperture r [cm]
Solenoid (0.6 [T])	29.6 (coil) 39.52 (iron)	7.75 (coil) 8.00 (iron)
ES Gap (50 [kV])	27.6	9.921 (upstream) 7.620 (downstream)
Bend (0.17 [T])	99.7456 (core) 63.5 (curvature)	20.5 (horizontal) 5.0 (vertical)

The iron bending magnet is modeled with Opera [6] (electromagnetic design software) in 3D. Figure 2(a) shows the vertical dipole field B_y on longitudinal axis ($x = 0$ and $y = 0$) along the center-line of the element, and Fig. 2(b) shows the variation of B_y as a function of the radial coordinate x at the element center ($y = 0$ and $z = 3.047$). B_y varies due to slanted iron poles of the magnet. This magnet has significant nonlinearity and an extended fringe field.

Uranium Beam Emerging from ECR

A multi-species beam emerges from the ECR with U with $Q = 25$ to 40 and O (from support gases) with $Q = 1$ to 4 [2]. Two desired “target” species to retain are U^{33+} and U^{34+} . Table 2 summarizes parameters applied to all species emerging from the ECR source. This normalized canonical angular momentum and normalized thermal rms emittance of U^{33+} corresponding to these parameters are 0.381 mm-mrad and 0.042 mm-mrad, respectively.

Table 2: Simple Symmetric Ion Distribution

Initial distribution	Waterbag
Ion temperature	3.0 [eV]
Magnetic field at ion birth	1.65 [Tesla]
RMS size (x, y)	(2.0, 2.0) [mm]
Neutralization factor	75 [%]

PIC SIMULATIONS

In our simulations, we assume an initial Waterbag distribution including space-charge adaption for each charge state [7]. 2D slice (xy) Warp PIC simulations using the model described in Ref. [2] are carried out from the ECR source to before bending magnet. The xy distribution is then used to continuously inject a 3D distribution into the dipole to carry out 3D steady state simulations (advanced twice the $\sim 2 \mu\text{s}$ dipole transit time of the slowest species).

* fukushim@frib.msu.edu

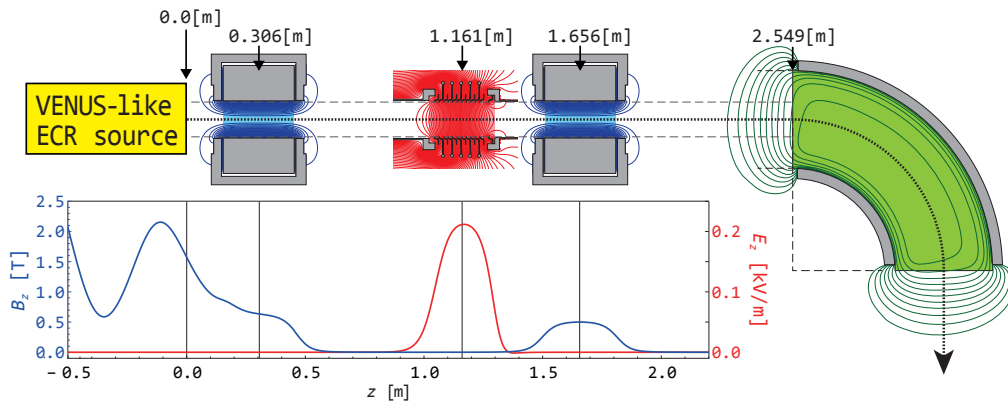


Figure 1: Lattice and on-axis field profiles.

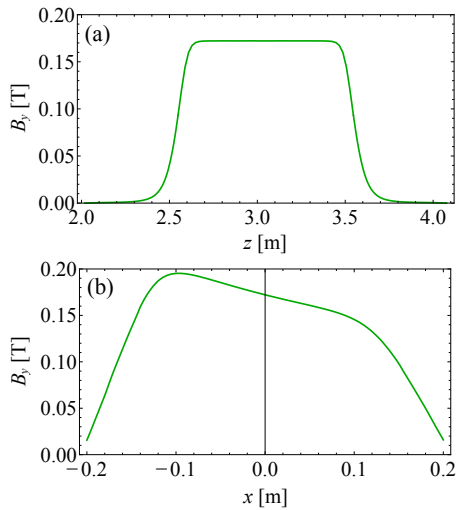


Figure 2: 3D bending magnet field (a) Bending field B_y on longitudinal axis ($x = 0.0$ [m]). (b) Bending field at the mid-plane of the bend ($z = 3.047$ [m])

Ideal (Sector) Bending Field

First, we modeled the dipole by an ideal sector dipole with no fringe and a flat B_y field. Figure 3 shows results from a Warp PIC simulation. Solid lines show the beam centroid of each charge. Corresponding rms beam envelope extents (shaded regions) are indicated for U^{32+} , U^{33+} , and U^{34+} . The dipole strength is adjusted so that U^{33+} is the reference species so this component has centroid $x = 0$. The beam envelopes are focused by the bending magnet. No focusing changes from slanted dipole poles is included.

3D Bending Field

Next, we import the 3D field map of the dipole with slanted poles into the simulation. This is carried out by transforming the field to the bent coordinate system defined by a design reference particle in an ideal sector bend. The best placement and dipole strength (consistent with the extended fringe) is found such that the reference species emerges at $x = 0$. We define a radial center shift Δr as the displacement

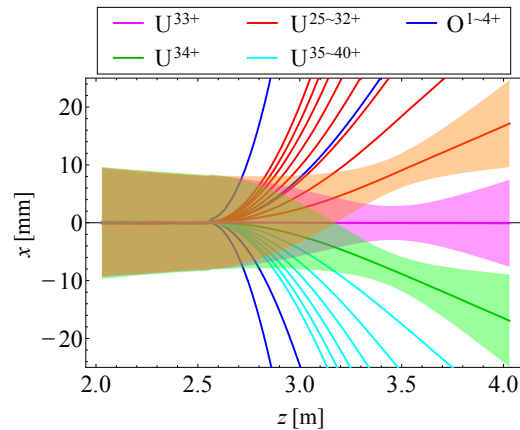


Figure 3: Beam centroids and rms envelopes in an ideal sector dipole from a PIC simulation with space-charge.

of the mid-plane center line and a dipole strength scaling factor α (measured from B_y at $x = 0$ and the axial center relative to sector bend value). For an incident design particle (initial $x = 0$) to emerge on-axis ($x = 0$), a numerical root finding procedure using single-particle simulation data finds that $\Delta r = 1.245 \times 10^{-4}$ mm and $\alpha = 1.00185$. Figure 4 shows the corresponding design particle coordinate and angle evolution in the dipole. Dashed curves correspond to the results obtained if the magnet placed on geometric center ($x = 0$) with no scale shift ($\alpha = 1$). Because the values of Δr and $1 - \alpha$ are so small, the magnet should be placed at the geometric center and any residual centroid errors corrected with appropriate upstream and downstream dipole steering.

Figure 5 shows the PIC simulation corresponding to Fig. 4. The reference species (U^{33+}) centroid emerges about ~ 0.3 [mm] off-axis. This small shift shows that the effect of non-reference self-field components altering the target centroid relative to the ideal case are relatively small. Note that beam focusing is altered due to the slanted poles of the dipole.

Neutralization Factor Dependence

A neutralization factor of 75 % was employed in the previous simulations. However, the actual neutralization factor

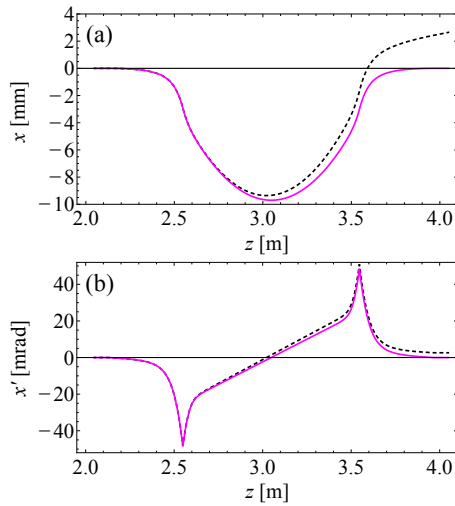


Figure 4: Reference species (U^{33+}) design particle coordinate (a) and angle (b) in the 3D dipole field from single-particle simulations. The optimized beam position at the end of the dipolefield is $(x, y) = (1.2 \times 10^{-8}, 4.4 \times 10^{-12})$ [mm] and $(x', y') = (3.0 \times 10^{-10}, 4.1 \times 10^{-12})$ [mrad].

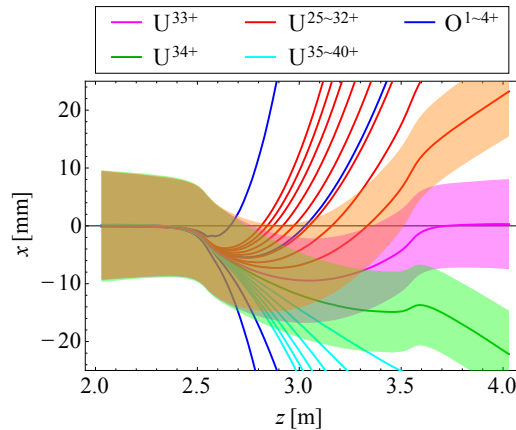


Figure 5: Beam centroids and rms envelope in a 3D dipole with slanted poles from a PIC simulation with space-charge.

is unknown and is likely varying. To simply test sensitivity, results of simulations with different uniform neutralization factors are shown in Fig. 6. Figure 6(a) shows the transverse phase-space projections of U^{33+} in the case of 75 % neutralization (same as Fig. 5). Figure 6(b) shows the case of zero neutralization factor (full space charge). The beam distribution becomes strongly distorted with lower neutralization factors and significant beam halo is generated in the worst (full space charge) case. There is significant x - y beam rotation due to canonical angular momentum.

CONCLUSION

We have carried full-3D simulations of the beam emerging from an ECR source through the first dipole bending magnet with slanted poles. Studies of optimal dipole placement suggest that the best strategy is to simply place the 3D dipole at the geometric center, adjust excitation to bend, and steer any

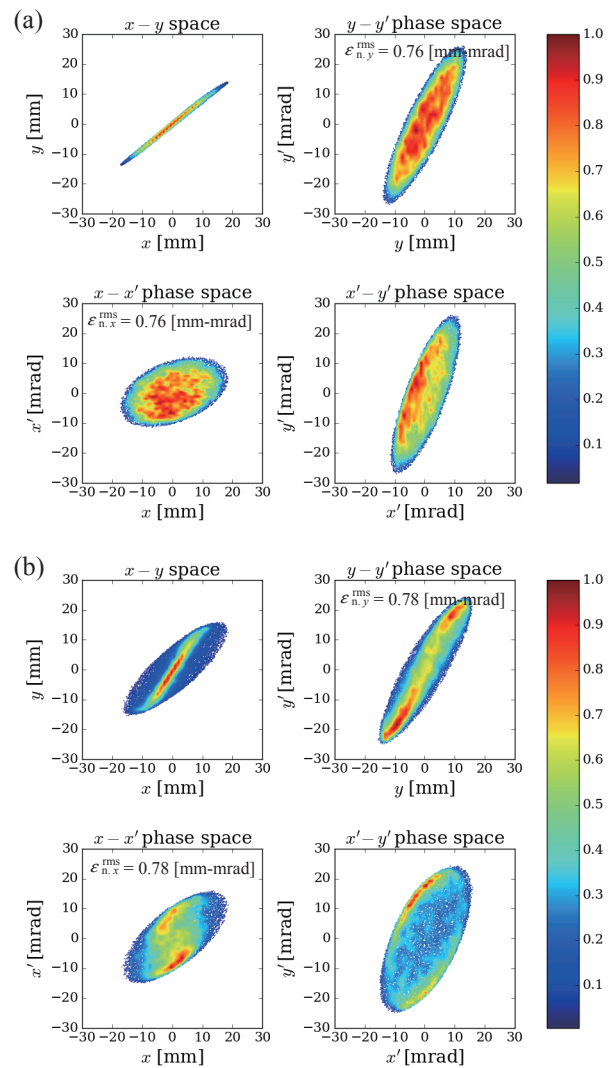


Figure 6: Phase-space distribution projections of U^{33+} at the exit of the bend section ($z = 4.03$ [mm]). for (a) 75%, and (b) 0% (full space charge) neutralization factors. Corresponding normalized rms emittance values are indicated.

residual error because center (Δr) and strength (α) adjustments would require placement within $\Delta r \sim 0.1 \mu\text{m}$ and α accurate to within $\sim 0.1\%$ for the reference species centroid to emerge on-axis closer than $x \sim 3$ mm and $x' \sim 3$ mrad. 3D space charge effects in bending section have been characterized and the space charge “push” on the target species centroids for Uranium appears to result in less than 1 mm amplitude error. This small value likely results from a near cancellation of pushes in competing directions by ultimately collimated species. The beam envelope and phase-space distortions in the bend are found to strongly vary with initial conditions and especially the neutralization factor.

ACKNOWLEDGMENTS

Work supported by the U.S. DOE Office of Science under Cooperative Agreement DE-SC0000661 and the NSF under Grant No. PHY-1102511.

REFERENCES

- [1] Warp web site, <http://warp.lbl.gov/> .
- [2] S. M. Lund, E. Pozdeyev, H. Ren, and Q. Zhao, “RMS Emittance Measures for Solenoid Transport and Facility for Rare Isotope Beams Front-end Simulations”, in *Proc. HB’14 Michigan USA*, November 2014, paper MOPAB17.
- [3] C. Y. Wong, K. Fukushima, and S. M. Lund , “Self-Consistent PIC Modeling of Near Source Transport of FRIB”, presented at Linac’16, Michigan USA, September 2016, paper TUPRC014.
- [4] G. Machicoane, N. Bultman, G. Morgan, E. Pozdeyev, X. Rao, J. Benitez, C. Lyneis, and L. T. Sun, “Design Status of ECR Ion Source and LEBT for FRIB”, in *Proc. ECRIS’12*, Sydney, Australia, September 2012, paper THY003.
- [5] Poisson/Superfish web site, http://laacg.lanl.gov/laacg/services/download_sf.shtml
- [6] Opera software web site, <http://operafea.com/>
- [7] S. M. Lund, T. Kikuchi, and R. C. Davidson, “Generation of Initial Kinetic Distribution for Simulation of Long-Pulse Charged Particle Beams with High Space-Charge Intensity”, *Phys. Rev. ST Accel. Beams* **12** (2009) 114801.